Quantitative sensory testing response patterns to capsaicin- and ultraviolet-B–induced local skin hypersensitization in healthy subjects: a machine-learned analysis

Jörn Lötsch[a,b,*], Gerd Geisslinger[a,b], Sarah Heinemann[a], Florian Lerch[b,c], Bruno G. Oertel[a,b], Alfred Ultsch[c]

Abstract

The comprehensive assessment of pain-related human phenotypes requires combinations of nociceptive measures that produce complex high-dimensional data, posing challenges to bioinformatic analysis. In this study, we assessed established experimental models of heat hyperalgesia of the skin, consisting of local ultraviolet-B (UV-B) irradiation or capsaicin application, in 82 healthy subjects using a variety of noxious stimuli. We extended the original heat stimulation by applying cold and mechanical stimuli and assessing the hypersensitization effects with a clinically established quantitative sensory testing (QST) battery (German Research Network on Neuropathic Pain). This study provided a 246×10-sized data matrix (82 subjects assessed at baseline, following UV-B application, and following capsaicin application) with respect to 10 QST parameters, which we analyzed using machine-learning techniques. We observed statistically significant effects of the hypersensitization treatments in 9 different QST parameters. Supervised machine-learned analysis implemented as random forests followed by ABC analysis pointed to heat pain thresholds as the most relevantly affected QST parameter. However, decision tree analysis indicated that UV-B additionally modulated sensitivity to cold. Unsupervised machine-learning techniques, implemented as emergent self-organizing maps, hinted at subgroups responding to topical application of capsaicin. The distinction among subgroups was based on sensitivity to pressure pain, which could be attributed to sex differences, with women being more sensitive than men. Thus, while UV-B and capsaicin share a major component of heat pain sensitization, they differ in their effects on QST parameter patterns in healthy subjects, suggesting a lack of redundancy between these models.

Keywords: Quantitative sensory testing, Human experimental pain models, Heat pain, Cold pain, Pressure pain, Sex differences, Subgroup identification, Machine-learning, Data science, Neuronal networks

1. Introduction

Biomedical research using cell experiments, laboratory animals, or human volunteers often produces complex multidimensional data. The complex trait of pain, which is known to rely on a complex network of molecular nociceptive pathways,[34] results in a similarly complex phenotypic representation.[55] Therefore, the assessment of pain-related human phenotypes requires detailed diagnostic approaches.[4,7,28] Consequently, combinations of

several experimental nociceptive stimuli are used to address particular sensory attributes or different neuronal and molecular mechanisms of nociception or analgesia.[77] Standardized quantitative sensory testing (QST) protocols[71] use combinations of thermal and various mechanical stimuli to explore the spectrum of sensory abnormalities that often accompany neuropathic pain.[95]

Human pain research, based on the exploration of pain phenotypes with batteries of diagnostic tests, routinely produces complex biomedical data. The influence of different factors on the pain phenotype may result in a highly complex distribution of the data, and as a consequence, complex data analysis methods are required. Recent developments in computational and data science offer a multidisciplinary collaborative approach for extracting pertinent information from biomedical data and generating knowledge from that information.[67] These developments include machine-learning methods that structure the biomedical data into clusters.

In this study, we acquired complex data by experimentally inducing pain in healthy subjects[26] by using 2 different hypersensitization procedures established in human experimental pain research, consisting of application of ultraviolet-B (UV-B) or topical capsaicin to a small area of skin. We analyzed the effects of these treatments on the parameters of a QST battery using machine-learning[58] and feature selection[24] techniques, which provide a set of methods that can automatically detect patterns in data or perform other kinds of decision making under conditions of uncertainty.[58] The main classical types of machine

learning, supervised and unsupervised learning (Box 1), were primarily used to explore data and to identify the QST parameters that are most affected by the hypersensitization procedures.

2. Methods

2.1. Subjects and study design

The study protocol complied with the Declaration of Helsinki on Biomedical Research Involving Human Subjects and was approved by the Ethics Committee of the Medical Faculty of the Goethe University, Frankfurt am Main, Germany (protocol number 28/11). Healthy volunteers who considered themselves to be of Anglo-American ethnicity (n = 100, 46 men), aged 19 to 42 years (mean ± standard deviation 25 ± 3.5 years), were enrolled after providing informed written consent. Exclusion criteria were drug intake during the previous week (except for oral contraceptives, vitamins, or hormone substitutes such as L-thyroxin), a current clinical condition involving pain, and current diseases, according to questioning and medical examination. Prior to the experimental tests, all subjects completed training sessions with pain tests applied to an area different from the planned test and control areas.

2.2. Application of experimental hypersensitization (treatments)

Experimental local hypersensitization of the skin was induced by either applying UV-B[80] or capsaicin cream[65] topically on the inner part of the subject's forearm. The application sides (left or right) of either model were randomized among subjects, with equal proportions of men and women in each treatment subgroup.

The UV-B pain model uses UV light to induce a small area of inflammation, allowing the assessment of mechanical and thermal thresholds.[23,27,30] Irradiation of the skin was performed inside the forearm on an area without any superficial veins or birth marks, in a different area than was used in the experiments to assess hyperalgesia. First, to determine the minimal erythema dosage (MED), 6 areas of 1 cm^2 were irradiated at a cumulative UV-B dosage between 200 and 600 mW/cm^2 (UV-B lamp UV 109; Waldmann Medizintechnik, Villingen-Schwenningen, Germany). The lamp was placed at a distance of 2.5 cm from the skin. UV-B dosage was increased by extending the irradiation time. Minimal erythema dosage was determined as the smallest dosage that led to a visual reddening of the irradiated area of skin after 24 hours. Subsequently, for the actual experiments, a different area of skin on the inner forearm was chosen according to the same criteria as used for MED determination. This area was irradiated with double the MED, and the experiments were performed 24 hours after UV-B irradiation.

In the capsaicin experimental pain model, chemical methods of nociceptor stimulation were used to produce stable and long-lasting hyperalgesia with a low potential for skin injury, in the original publication supplemented by heat stimulation[65] and in this study with additional cold and mechanical stimuli. In this study, 150 mg of capsaicin cream (0.2%, manufactured by the local hospital pharmacy) was topically applied to a 3 × 3-cm^2 area of skin. Subsequently, the area was covered with a plaster for 30 minutes before the QST parameters were acquired.

2.3. Quantitative sensory testing and raw data processing

Quantitative sensory testing was performed twice in each subject, once at baseline and again following application of experimental hypersensitization. A clinically established QST test battery was used as proposed by the German Research Network on Neuropathic Pain.[71,72] This battery includes thermal and mechanical stimuli grouped into 7 tests of sensory perception and pain (Table 1) administered in the following order: thermal testing, mechanical detection threshold, mechanical pain threshold, mechanical pain sensitivity, temporal pain summation, vibration detection threshold (VDT), and pressure pain threshold (PPT). The room temperature was kept at 20 to 25°C during testing. Measurements were taken by trained investigators fully adhering to previously published instructions,[66,71,72] which are briefly recapitulated in Table 1.

The 7 tests provided a total of 13 different QST parameters, which were processed according to the published instructions,[66,71,72] including log-transformation of some parameters as specified in Table 1, in the column headed "Basic data processing." Subsequently, each QST parameter value was mapped onto the distribution of a reference group consisting of a total of 180 healthy subjects, in whom a data set of 1080 values was obtained. This map serves as the reference for all QST-based diagnoses.[48] Therefore, according to the standard QST procedure, the individual QST parameter values were z-transformed as

$$z_{QST,individual} = \frac{QST_{individual} - QST_{reference}}{Standard\ deviation_{reference}},$$

where the QST reference values and standard deviations were values published in a methodological article[48] with regard to the subject's sex, age, and body site tested. The signs of the z-scores were adjusted to denote that a score >0 indicates high sensitivity and a score <0 indicates low sensitivity, according to the standard instructions.

2.4. Data analysis

Complete data were obtained from 82 subjects. Following the exclusion of differences between left-hand and right-hand sides in the baseline measurements, which was supported by nonsignificant

---

Text box 1. Overview on the main classical types of machine learning comprising supervised or unsupervised learning.

For supervised machine learning, the data space D = $\{(x_i, y_i)|x_i \in X, y_i \in Y, i = 1...n\}$ with a predefined division into an input space X and an output space Y. The input space comprises vectors $X_i < , X_i, 1, ...X_i, d > \subset \mathbb{R}^d$ >0 different parameters acquired during a study for n >0 cases. The output space Y comprises $y_i \in C = \{1,...,c\}$, where c denotes the possible classes such as treatment groups or diagnoses. During learning, the data space is searched with the aim of identifying an intelligent algorithm that maps the input features to the output classes. By contrast, for unsupervised machine learning, the data space $D_u = \{x_i | x_i \in X, i = 1...n\}$ lacks class information, and the task is to find interesting structures in the d-dimensional feature space $D_u \subset R^d$, which subsequently can be topically interpreted. In this study, both classes of machine-learned analysis were applied (1) to identify the most relevant effects of UV-B and topical capsaicin on quantitative sensory testing (QST) parameters and (2) to identify possible subgroups of subjects who share similar QST responses to the selected hypersensitization treatments.

The unsupervised machine-learning method used was the ESOM/U-matrix, which is a topology-preserving artificial neuronal network (Kohonen SOM[38,39]) used to project high-dimensional data points $x_i \in R^D$ onto a 2-dimensional self-organizing network consisting of a large grid of neurons.[88] Training for this unsupervised model means adapting to the structures of the high-dimensional input data. On top of the trained ESOM, the distance structure in the high-dimensional feature space was visualized in the form of a U-matrix. This visualization displays the distances between the points in the high-dimensional space in a color-coded manner using a geographical map analogy where large "heights" represent large distances in the feature space while low "valleys" represent data subsets that are similar. "Mountain ranges" with "snow-covered" heights visually separate the clusters in the data.[82,88]

Table 1

Components of the quantitative sensory testing battery of the German research network on neuropathic pain.[71,72]

Test		Quantitative sensory testing parameter	Sensory dimension assessed	Basic data processing
Thermal testing	CDT	Cold detection threshold	Application of cold stimuli on a 3×3-cm^2 skin area, baseline t° = 32°C, decreasing temperature ramp of 1°C/s, TSA 2001-II (MEDOC, Ramat Yishai, Israel)	Difference from baseline 32°C of the mean of 3 measurement repetitions; log-transformation
	WDT	Warmth detection threshold	Application of warm stimuli to a 3×3 cm^2 skin area, baseline t° = 32°C, increasing temperature ramp of 1°C/s, TSA 2001-II (MEDOC, Israel)	Difference from baseline 32°C of the mean of 3 measurement repetitions; log-transformation
	TSL	Thermal sensory limen	Application of alternating cold and warm stimuli to a 3×3-cm^2 skin area, baseline t° = 32°C, temperature ramp of 1°C/s, TSA 2001-II (MEDOC, Israel)	Difference in the means of the 3 warmth and the 3 cold detection thresholds; log-transformation
	CPT	Cold pain threshold	Application of cold stimuli to a 3×3 cm^2 skin area, baseline t° = 32°C; decreasing temperature ramp 1°C/s, TSA 2001-II (MEDOC, Israel)	Mean of the 3 measurement repetitions
	HPT	Heat pain threshold	Application of warm stimuli to a 3×3-cm^2 skin area, baseline t° = 32°C, increasing temperature ramp of 1°C/s, TSA 2001-II (MEDOC, Israel)	Mean of the 3 measurement repetitions
Pressure pain threshold	PPT	Pressure pain threshold	Application of blunt pressure stimuli to musculus thenar for the hand area and musculus abductor hallucis for the foot area, Commander Algometer, JTECH Medical, Midvale, Utah (1 cm^2 probe area)	Mean of the 3 measurement repetitions; log-transformation
Mechanical pain threshold	MPT	Mechanical pain threshold	Application of pinprick stimuli (forces 8-512 mN; contact area 0.2 mm) following staircase paradigm, starting force of 8 mN, the Pin-Prick, MRC Systems GmbH, Heidelberg, Germany	Geometric mean of the 5 ascending and 5 descending stimuli; log-transformation
Stimulus-response function	MPS	Mechanical pain sensitivity for pinprick stimuli	Application of pinprick stimuli and tactile stimuli in a balanced order, pain rating of each pinprick stimulus on a 0 to 100 numerical rating scale ("0" = "no pain," "100" = "strongest pain imaginable"), the Pin-Prick, MRC Systems GmbH, Heidelberg, Germany	Geometric mean of the pain ratings of the 35 pinprick stimuli; log-transformation
Wind-up	WUR	Wind-up ratio	Temporal summation of pinprick stimuli, application of single pinprick stimulus (force 256 mN) followed by train of 10 pinprick stimuli (force 256 mN, 1/s repetition rate) over skin area of 1×1 cm^2, pain rating of the train on a 0 to 100 numerical rating scale ("0" = "no pain," "100" = "strongest pain imaginable"), the Pin-Prick, MRC Systems GmbH, Heidelberg, Germany	Ratio of the mean pain ratings of the 5 series of stimuli and the mean pain ratings of the 5 single stimuli; log-transformation
Mechanical detection threshold	MDT	Mechanical detection threshold	Application of von Frey hairs (forces 0.25-512 mN, diameter 0.5 mm) following stare-case paradigm, starting force of 16 mN, Optihair2-Set, MARSTOCK nervtest, Schriesheim, Germany	Geometric mean of the 5 ascending and 5 descending stimuli; log-transformation
Vibration detection threshold	VDT	Vibration detection threshold	Application of descending vibration stimuli (Rydel-Seiffer tuning fork, 64 Hz, 8/8 scale) to the processus styloideus radii for the hand area and malleolus medialis for the foot area	Mean of the 3 measurement repetitions

paired t tests[79] performed for each QST parameter, transformed baseline data (z-values) were averaged between the 2 test sides. As observed previously,[18,45] the QST parameters dynamic mechanical allodynia and paradoxical heat sensations did not vary among the subjects, and the QST parameter vibration detection threshold displayed only 2 different values in the whole cohort (0 or 1) that did not change following application of the hypersensitization procedures. Therefore, these parameters were omitted from the analyses.

The analyzed data set consisted of 10 QST parameters acquired in 82 healthy subjects in the 3 study conditions

(treatments): (1) baseline, (2) following application of UV-B, and (3) following topical application of capsaicin. The z-transformed QST parameter values obtained according to the standard procedure of the QST battery[48] provided the data space $D = \{(x_i, y_i)|x_i \in X, \ y_i \in Y, \ i = 1...82\}$. The cases $x_i \in X$ were the QST parameters acquired from the volunteers in our study, and the output space Y comprising $y_i \in C = \{1,2,3\}$ was given by the 3 different study conditions. This data space was analyzed using machine-learning[58] and feature selection techniques[24] to (1) identify the QST parameters most affected by the hypersensitization treatments and (2) explore the data space for high-dimensional structures associated with the hypersensitization conditions or with subject subgroups sharing similar responses to the hypersensitization treatments. Finally, (3) the key results of the machine-learned analysis were verified by comparing them with the results of a standard variance analytical approach.

All analyses were performed using the R software package (version 3.3.3 for Linux; http://CRAN.R-project.org/, Ref. 68) on an Intel Xeon computer running on Ubuntu Linux 16.04.2 64-bit. The steps of the machine-learned analysis are described in detail as follows.

2.4.1. Machine-learned analysis to identify the quantitative sensory testing parameters most affected by hypersensitization

To identify the QST parameters that were most affected by UV-B or topical capsaicin application, we started with the hypothesis that these parameters can provide the basis for the correct association of a measurement with the hypersensitization treatments under which the data had been acquired. We approached this task using supervised machine learning. Our analysis included (1) a feature selection step, which aimed at identifying the most relevant QST parameters (features) for correct assignment to different classes or treatments, which was followed by (2) creation of a classifier that allowed us to explore differences in the effects of the hypersensitization treatments.

2.4.1.1. Feature selection

The QST parameters differing most relevantly among the 3 experimental conditions, and thus qualifying as basis by which to distinguish the study conditions, were identified using techniques of unsupervised machine learning[58] and feature selection.[24] Specifically, the input-output pairs $D = \{(x_i, y_i)|x_i \in X, \ y_i \in Y, \ i = 1...82\}$ were submitted to random forest machine learning. A random forest consists of a set of different, uncorrelated, and often very simple decision trees.[9] Each decision tree uses a tree data structure with conditions on variables (parameters) as vertices and classes as leaves. Each tree in the random forest votes for a class. The final classification assigned to a data point follows the majority of these class votes.

In our analysis, in 1000 repeated experiments the original data set was split into 2/3 training and 1/3 test data subsets, by means of class-proportional bootstrap resampling from the training data set[20] using the R library "sampling" (https://cran.r-project.org/package=sampling, Ref. 83), to increase the robustness of the analysis. For each of the 1000 experiments, 500 random decision trees were created, each tree containing $d \in \{1,...,10\}$ features randomly drawn from the d = 10 QST parameters. The number of trees was based on visual analysis of the relationship between the number of decision trees and the accuracy of the classification. This analysis indicated no improvement beyond approximately 300 trees; therefore, building 500 trees was considered to

provide robust results. Within this analysis, bootstrap resampling was used again to split the training data subset into further training and test subsamples, and trees were created on these training subsamples and applied to test subsamples. Thus, the whole analysis accommodated the concept of a nested cross-validation analysis,[93] with the inner loop consisting of the decision tree analysis on data resampled from the training data subset and the outer loop consisting of the 1000 splits of the whole data set into training and test data. The trees were analyzed with respect to the features included and the accuracy of classification into the 3 treatment groups. For each feature, we computed the mean decrease in Gini impurity (https://en.wikipedia.org/wiki/Decision_tree_learning#Gini_impurity) while excluding the respective parameter from a random forest building. We thus provided a rating criterion for the importance of each QST parameter to serve as a basis to conclude the experimental condition, under which its value had been acquired, ie, the amount of this decrease indicated the importance of the particular feature. We performed these calculations using the "randomForest" library (https://cran.r-project.org/package=randomForest, Ref. 44).

Following each of the 1000 random forest analyses on resampled data, we submitted the values of the mean decreases in Gini impurity to computed ABC analysis while excluding the parameter from random forest analysis.[87] ABC analysis is a categorization technique for selection of the most important subset among a larger set of items, and we chose it because it fit the basic requirements of feature selection using filtering techniques,[75] ie, it easily scales to very high-dimensional data sets, is computationally simple and fast, and is independent of the classification algorithm. ABC analysis aims at dividing a set of data into 3 distinct subsets called "A," "B," and "C." Set A should contain the "important few," ie, those elements that allow us to obtain a maximal yield with a minimal effort.[35,62] Set B comprises those elements where an increase in effort is proportional to the increase in yield. By contrast, set C contains the "trivial many," ie, those elements with which the yield can only be achieved with a disproportionally great additional effort.[35,62] The target QST parameters for further exploration of the hypersensitization effects were sought in ABC set "A." The final size of the feature set was equal to the most frequent size of set "A" in the 1000 runs. The final members of the feature set were chosen in decreasing order of their appearances in ABC set "A" among the 1000 runs. These calculations were done using our software package (http://cran.r-project.org/package=ABCanalysis, Ref. 87).

2.4.1.2. Explorative analysis to identify the quantitative sensory testing parameters most affected by hypersensitization

The QST parameters most frequently assigned to set "A" in the 1000 random forests and ABC analysis of resampled data, at the number corresponding to the most frequent size of set "A," were used to create a decision tree associating ranges of QST parameter values with the 3 study conditions. This tree was obtained by means of decision tree learning using the classification and regression tree algorithm.[10] As in random forests, a tree data structure is created with conditions on variables (parameters) as vertices and classes as leaves. In random forests, tree structure is randomly created, making it impossible to interpret single trees, but in classical decision trees, local decisions follow statistical criteria and aim at providing a simple and easily understandable set of classification rules suitable for topical interpretation, which is why we chose to use them in the present exploratory analysis. We used the concept of Gini impurity to find optimal (local)

mutually exclusive decisions. The calculations used the "ctree" function of the "party" software package (https://cran.r-project. org/package=party, Ref. 32). We assessed the significance of the splits at each decision node by applying permutation tests as implemented in the "ctree" function. Nodes were only split if the null hypothesis of independence between the response variable, ie, the treatment class, and the predictors, ie, the QST parameter values, could not be rejected at the given level of significance. Finally, we assessed the performance of the identified decision tree to correctly assign the treatment during which data had been acquired by calculating the overall classification accuracy of treatment assignment using standard equations.[2] We repeated these steps in 1000 runs of randomly resampled data subsets class—proportionally drawn from the complete data sets. The accuracy was the median of the values obtained in the 1000 runs, and the 95% confidence interval spanned between the 2.5th and 97.5th percentiles of the range of the 1000 associated accuracy values.

2.4.2. Machine-learned analysis of quantitative sensory testing parameter–based data structures

To identify response patterns of QST parameters to the hypersensitization treatments, we analyzed the baseline values together with parameters acquired after application of UV-B or capsaicin. We performed this analysis in 4 main steps, comprising (1) data preprocessing based on Bayesian statistics; (2) detection of distance- and density-based data structures based on emergent self-organizing maps followed by subgroup detection; (3) decision tree–based exploration of the QST parameter pattern of the data cluster structure we had obtained; and (4) topical characterization of the data structures, including sex differences.

2.4.2.1. Data preprocessing

The 10 × 246 matrix, we obtained (10 z-transformed QST parameters acquired in 82 subjects under 3 different treatments comprising baseline, UV-B, and capsaicin), provided the data space $D = \{x_i, i = 1, ..., 82\} \subset \mathbb{R}^{10}$. We analyzed the parameters (features) with respect to their probability density function. We did so by applying the Pareto density estimation (PDE), which is a kernel density estimator particularly suitable for the discovery of groups.[86] For each of the 10 QST parameters, the magnitudes were described as either low, average, or high, reflecting the previous phenotypes of "low pain sensitivity," "average pain sensitivity," and "high pain sensitivity" proposed by Diatchenko et al.[17] The association of each value to 1 of the 3 classes was obtained by means of Gaussian mixture modeling. That is, the PDE was described as

$$p(x) = \sum_{i=1}^{M} w_i N(x|m_i, s_i) = \sum_{i=1}^{M} w_i \cdot \frac{1}{\sqrt{2\pi}s_i} \cdot e^{-\frac{(x-m_i)^2}{2s_i^2}},$$ where N (x| m_i, s_i) denotes Gaussian probability densities (component, mode) with means, m_i, and standard deviations, s_i, while w_i denotes the mixture weights controlling the relative contribution of each Gaussian component to the overall distribution, which add up to a value of 1, and M = 3 denotes the number of components in the mixture corresponding to the 3 proposed classes described above (low pain sensitivity, average pain sensitivity, and high pain sensitivity). We fitted this model to the PDE of the data using our "AdaptGauss" software package (https://cran.r-project.org/ package=AdaptGauss, Refs. 43,90) and using the expectation maximization algorithm.[15] Subsequently, we calculated the probabilities for each data value to belong to each of the 3 Gaussian components as the Bayesian posteriors.[50] Finally, we subtracted the probabilities of belonging to the small data value

range from those of belonging to the high data value range, providing 10 vectors scaled in the interval [−1,...,1].

2.4.2.2. Detection of distance- and density-based data structures

The 10 × 246 matrix of Bayesian posteriors belonging to low, average, or high QST values within each parameter range across the whole study provided the unsupervised data space $D_u \subset [-1,1]^{10}$ that we explored for distance- and density-based structures. We performed this exploration by means of unsupervised machine learning.[58] The task was to identify data structures that reflected the treatments applied in the experiments and to suggest possible subgroups of responders to the treatments. Machine learning was implemented as emergent self-organizing feature maps (ESOMs)[38] that were combined with the U-matrix.[85] This method has been shown to provide an unbiased way to identify structures in biomedical data.[88] Specifically, ESOMs are based on a topology-preserving projection of high-dimensional data points $x_i \in R^D$ onto a 2-dimensional self-organizing network consisting of a grid of neurons. This approach represents a topology-preserving mapping of high-dimensional data points onto a 2-dimensional grid of neurons that therefore favored more common clustering algorithms such as k-means, Ward, complete, and average linkage,[47] which in contrast to the ESOM/U-matrix method are prone to detect false structures in the data.[88] The neural network consisted of a 2-dimensional toroid grid[85] of so-called neurons with 50 rows and 80 columns (n = 4000 units; for SOM size determination, see Ref. 88). Each neuron holds, in addition to a position vector on the 2-dimensional grid, a further vector carrying "weights" of the same dimensions as the input dimensions. The weights were initially randomly drawn from the range of the data variables and were subsequently adapted to the data during the learning phase that used 30 training cycles.

After training of the neural network, we obtained an ESOM that represented the subjects on a 2-dimensional toroid map as the localizations of their respective "best matching units" (BMU), which are neurons on the grid that after ESOM learning carried the vector that was most similar to a subjects' data vector. On top of this grid, the distances between data points are calculated with the U-matrix.[47,89] Every value (height) in the U-matrix depicts the average high-dimensional distance of a prototype to all immediate neighboring prototypes regarding a grid position. The U-matrix can be enhanced by calculating a P-matrix[85] displaying the point density for a neuron m_j as $p(m_j) = |\{$data points $x_i \in D | d(x_i, w(m_i)) < r > 0, r \in \mathbb{R}\}|$, estimated as the number of data points belonging to the data space D in a sphere with radius r belonging to the real numbers $\mathbb{R}$ around the weight $w(j)$ of each neuron m_j on the ESOM's output grid. The U*-matrix combines distance structures (U-matrix) and density structures (P-matrix) into a single matrix.[85] The corresponding visualization technique is a topographical map with hypsometric colors,[81] facilitating the recognition of distance- and density-based structures. Large "heights" in brown and white colors represent large distances between data points (subjects) separating "valleys" in green and blue colors that represent data points that are similar.

2.4.2.3. Assessment of cluster structures and hypersensitization response subgroups

The ESOM/U*-matrix analysis provided a distance- and density-based cluster structure of the data of the complete study. That is, each treatment had been regarded as a separate data subset

leading to the representation of each subject 3 times on the ESOM with data points for each treatment. Therefore, cluster structures provided a basis to identify both (1) the effects of the hypersensitization treatments and (2) subgroups of subjects sharing response patterns to the treatments.

To explore the cluster structure, we submitted the z-values of the QST parameters to decision tree learning as described above, ie, using the classification and regression tree algorithm[10] with the Gini impurity as basis of a dichotomous split criterion to find an optimum as implemented in the "ctree" function of the "party" package (https://cran.r-project.org/package=party, Ref. 32). An α-level of $P = 0.001$ was chosen for split significance and was corrected for multiple testing according to the procedure proposed by Bonferroni.[8] The performance of the identified decision tree to correctly assign a data point to its U*-matrix–based cluster was assessed by calculating the overall classification accuracy of treatment assignment as accuracy [%] = number of correct treatment associations/total number of treatment associations.[51]

We approached the interpretation of the cluster-specific QST pattern by associating the original hypersensitization treatments to the U*-matrix–based clusters. Therefore, we analyzed the treatment vs cluster contingency table with respect to over-representation or underrepresentation of treatments in clusters. Specifically, we obtained the permutation distribution of this 2-way table and calculated the sum of squares of the Pearson residuals as the test statistic of independence.[97] We assessed test significance using Pearson χ^2 test.[64] This step allowed us to associate particular study conditions (baseline, UV-B, and capsaicin) with U*-matrix clusters. These calculations were done using the "vcd" library (https://cran.r-project.org/package=vcd, Ref. 54).

In addition to exploring the U*-matrix–derived clusters for treatments effects, we also looked at cluster membership with respect to sex differences. Therefore, we submitted cluster membership vs sex cross-tables, obtained for study treatments, decision-tree analysis, and ESOM/U*-matrix analysis, to Fisher exact tests.[21]

2.4.3. Reassessment of key results using analysis of variance

To reassess key results of machine-learned analyses using classical statistical methods, we analyzed the effects of UV-B or topical capsaicin on QST parameters by submitting the QST parameter z-values to conventional analysis of variance for repeated measures (rm-ANOVA) with "hypersensitization" (UV-B or capsaicin) as a within-subjects factor and "sex" as a between-subjects factor. The analyses were performed separately for each QST parameter. Each rm-ANOVA was followed by the analysis pairwise treatment differences by means of paired t tests.[79] The α-level was set at 0.05 and corrected for multiple testing,[8] separately for each rm-ANOVA (ie, 3 t tests).

3. Results

The QST parameter values obtained during the baseline measurements did not significantly differ between the test sides (t tests: P always >0.05) and were therefore averaged to obtain the baseline condition data subset. For technical reasons, data from 18 subjects were incomplete. Moreover, the QST parameters dynamic mechanical allodynia and paradoxical heat sensations lacked intersubject variation, and VDT displayed only 2 different values (0 or 1), which suggested exclusion of these values from the analyses. With baseline QST parameters having been averaged

between the 2 test sides, the data we analyzed were based on 3280 QST parameter values obtained in 82 subjects when counting the data in a similar manner as in the report of the reference values of the QST test battery that mentioned 1080 QST parameter values obtained in 180 subjects.[48] The distribution of the z-transformed data is shown in **Figure 1**.

3.1. Quantitative sensory testing parameters most affected by ultraviolet-B– or topical capsaicin-induced hypersensitization

Supervised machine learning using 1000 random forest analyses (**Fig. 2**) of bootstrap resampled data indicated different contributions to correct treatment association for particular QST parameters. Specifically, only 4 different QST parameters (heat pain threshold, cold pain threshold, cold detection threshold, and thermal sensory limen) had been included in successful decision trees. In the ABC analyses (**Fig. 2**) that had followed each random forest analysis, set "A" comprising items that contribute most to the association with the study treatments took sizes of 0, 1, 2, or 3 QST parameters in 7, 517, 387, and 89 of the runs, respectively. Therefore, a set size of 1 QST parameter was chosen for further analysis, and the QST parameter most frequently assigned to set "A," ie, in 993 runs, was HPT (**Fig. 2**).

Decision tree analysis using the selected QST parameter (**Fig. 3**) provided an overall classification accuracy of 67.9% (cross-validated nonparametric 95% confidence interval obtained in 1000 resampling runs: 60.5%-75.3%), which was substantially above 33% chance of assigning a measurement to 1 of the 3 study conditions. However, it also provided 100 to 67.9 = 32.1% falsely classified data points. Exploration of the decision tree (**Fig. 3**) indicated that data acquired following topical application of capsaicin were almost always associated with high heat pain sensitivity, whereas data acquired during the baseline condition were almost always associated with low heat pain sensitivity. However, data acquired following UV-B treatment were partly found to be associated with medium heat pain, while a fraction of the data shared a decision node with baseline data indicating nonresponse to hypersensitization. The decision tree allowed only for statistically significant splits comprised 6 final nodes (**Fig. 3**). The distribution of study conditions was statistically highly significantly different across the terminal tree nodes (χ^2 statistics: $P < 2 \cdot 10^{-16}$).

3.2. Quantitative sensory testing parameter–based data structures

Unsupervised machine learning identified structures in the data space $D = \{x_i, i = 1, \ldots, 82\} \subset \mathbb{R}^{10}$ comprising the variables $d = 10$ QST parameters, x, acquired from 82 subjects. Following projection of the vector space onto a toroid grid of $50 \times 80 = 4000$ neurons and training of a self-organizing map, a U*-matrix visualization was displayed on top of this SOM (**Fig. 4**) that visualized distance- and density-based data structures. The resulting ESOM visualized large gaps in the data space by large U-heights, whereas data located in close vicinity in the high-dimensional space were placed in regions with low U-heights on the U*-matrix. The valleys and ridges allowed the identification of 4 major clusters in the QST data space acquired during the present study (**Fig. 4A, B**). The study conditions (baseline, UV-B, and capsaicin) were unevenly represented in the clusters, as indicated by highly significant χ^2 statistics ($P < 2 \cdot 10^{-16}$).

Specifically, data acquired during the baseline condition were overrepresented in the first cluster and underrepresented in the 3
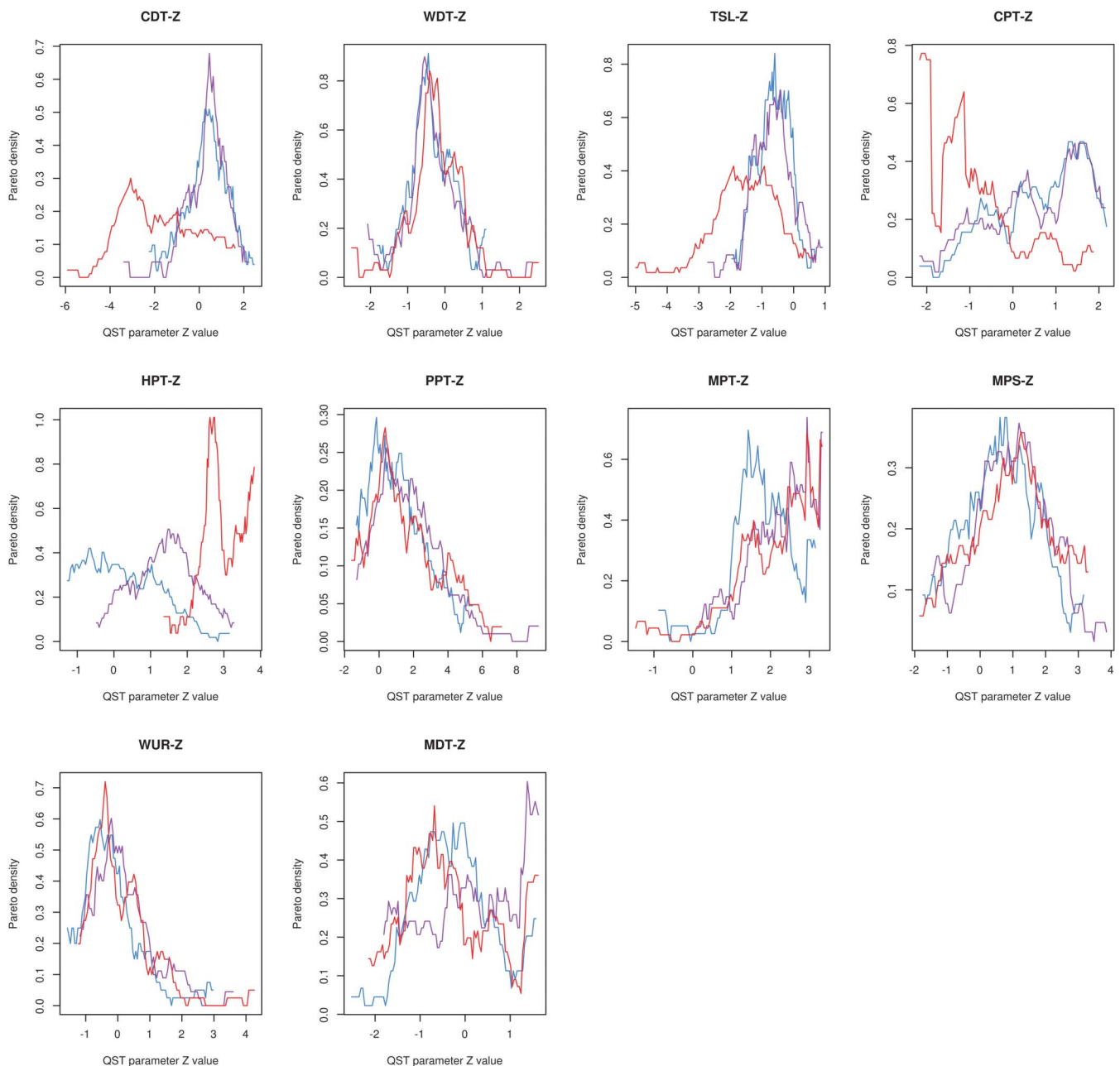
Figure 1. Distribution of the z-values of the quantitative sensory testing (QST) parameters at baseline (blue) and following hypersensitization induced by topical application of ultraviolet-B (violet), or capsaicin (orange-red). The density distribution is presented as probability density function (PDF), estimated by means of the Pareto density estimation ([86]black line). Higher z-scores indicate higher sensitivity to the respective stimuli. The figure was created using the R software package (version 3.3.3 for Linux; http://CRAN.R-project.org/, Ref. 68). CDT, cold detection threshold; CPT, cold pain threshold; HPT, heat pain threshold; MDT, mechanical detection threshold; MPS, mechanical pain sensitivity to pinprick stimuli; MPT, mechanical pain threshold; PPT, pressure pain threshold; TSL, thermal sensory limen; VDT, vibration detection threshold; WDT, warmth detection threshold; WUR, wind-up ratio.

other clusters (**Fig. 4D**). Indeed, cluster 1 comprised 74 of the 82 measurements acquired during the baseline condition. The first cluster was, however, larger than a third of the data points as it also contained 45 measurements acquired following application of UV-B hypersensitization. Given that further subclusters did not emerge in this cluster, this fraction of data acquired during the UV-B condition points at nonresponders to this treatment. Consistently, the second cluster that contained measurements acquired following UV-B treatment was comparatively small (n = 28 data points) and contained 19 measurements acquired during the UV-B condition. Finally, data acquired following topical application of capsaicin were overrepresented in 2 different

clusters in which all other study conditions were underrepresented (**Fig. 4D**). Indeed, 78 of the 82 measurements acquired following capsaicin application were located in clusters 3 or 4. The distribution on 2 different clusters indicated clear subgroups in the response to capsaicin hypersensitization.

Decision tree analysis of the U*-matrix–derived clusters (**Fig. 4C**), based on statistically significant data splits and providing an overall cluster association accuracy of 87.8% (95% CI: 83.05%-91.6%), indicated that again, heat pain sensitivity (QST parameter HPT) was the major distinctive criterion among the clusters as it had resulted in the supervised machine-learned analysis. However, additional QST parameters played
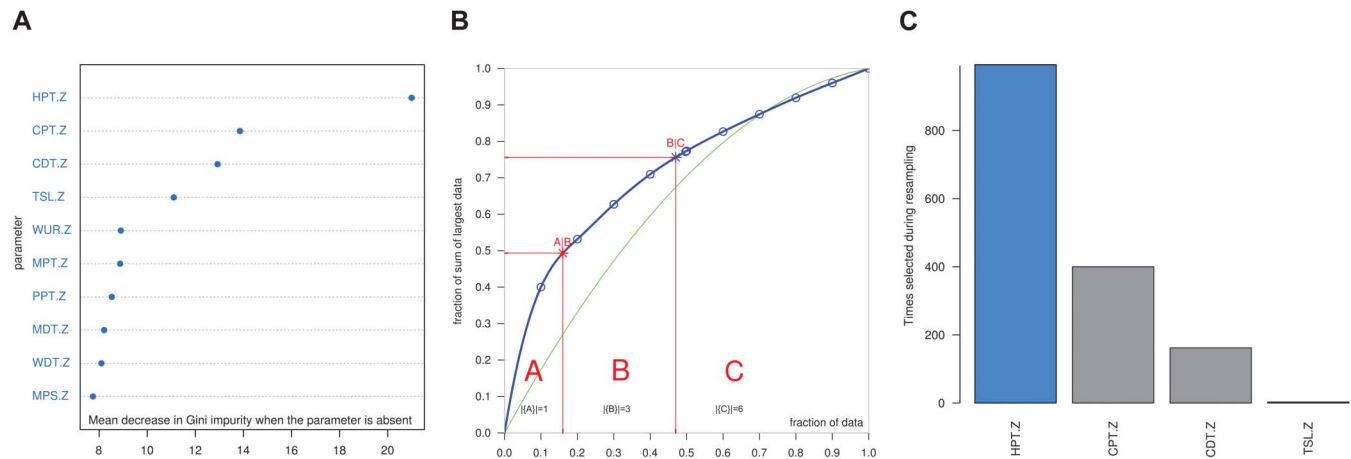
Figure 2. Machine-learned analysis to identify quantitative sensory testing (QST) parameters most affected by hypersensitization, implemented as random forest analysis followed by ABC analysis of the contribution of QST parameters to overall association of the measurements to the study treatments (baseline, ultraviolet-B, or capsaicin). (A) Dot chart[33] of the mean decrease in Gini impurity when the respective feature (QST parameter) is excluded from random forest decision tree building. The plot displays 1 typical example out of the analyses of 1000 bootstrap resampled data subsets. (B) Subsequent to random forest-based feature selection, the mean decrease in Gini impurity associated with each QST parameter was submitted to ABC analysis, which is an item selection procedure aiming at identification of the most profitable items from a larger list of items. The ABC plot (blue line) shows the cumulative distribution function of the mean decreases in accuracy, along with the uniform distribution (green line) in which each feature would have the same chance to contribute to the study condition assignment (for further details about computed ABC analysis, see Ref. 87). The red lines indicate the borders between ABC sets "A," "B," and "C." Only set "A," containing the most profitable item, was selected as the +relevant QST item subset. (C) Count of occurrences of QST parameters in ABC set "A" during the 1000 runs on bootstrap resampled data. The 4 parameters are those that ever appeared in set "A." Most frequently, the set size was |{A}| = 1 parameter and most often the QST parameter "HPT." Therefore, this parameter (blue) was selected as a sufficient basis for study treatment assignment during random forest–based feature selection for unsupervised machine-learned analysis. The figure was created using the R software package (version 3.3.3 for Linux; http://CRAN.R-project.org/, Ref. 68). In particular, the ABC analysis was performed and plotted using our "ABCanalysis" software package (http://cran.r-project.org/package=ABCanalysis, Ref. 87). CDT, cold detection threshold; CPT, cold pain threshold; HPT, heat pain threshold; MDT, mechanical detection threshold; MPS, mechanical pain sensitivity to pinprick stimuli; MPT, mechanical pain threshold; PPT, pressure pain threshold; TSL, thermal sensory limen; WDT, warmth detection threshold; WUR, wind-up ratio.

a role in correct cluster assignment. Specifically, high sensitivity to cold stimulation was important for assignment to the cluster containing the most data acquired following application of UV-B induced hypersensitization. By contrast, the 2 clusters to which most of the data acquired following application of capsaicin-induced hypersensitization were assigned could be distinguished by sensitivity to pressure pain (QST parameter PPT; **Fig. 4C**).

Thus, the difference in the response to capsaicin among subjects was mainly due to a different sensitivity to pressure pain. An analysis of the cluster membership vs sex cross-table (**Fig. 5**) indicated a different distribution of sexes among the U*-matrix–based clusters (Fisher exact test: $P = 0.009881$), in contrast to the original treatment vs sex distribution ($P = 1$) and to the sex distribution across the HPT-dependent decision tree nodes obtained in the supervised machine-learning analysis ($P = 0.2125$). This sex distribution prevailed between the 2 clusters associated with capsaicin treatment ($P = 0.03894$). Cluster 4, characterized by a higher sensitivity to pressure pain, contained more women than men, while the opposite was observed for cluster 3, characterized by a comparatively lower sensitivity to pressure pain. Thus, unsupervised machine-learned analysis followed by knowledge discovery using decision tree analysis pointed at a higher sensitivity to pressure pain in women as compared to men, which was reflected in the projection of the high-dimensional data space onto a toroid SOM.

### 3.3. Reassessment of key results using analysis of variance

Standard statistical analysis of the data indicated that the treatments exerted significant effects on all QST parameters except for warmth detection threshold, as indicated by the significance pattern of the results of the rm-ANOVA (**Table 2**). The significance pattern also indicated that the 2 treatments (UV-B or capsaicin) had influenced different QST parameters (**Table 2**). Moreover, the ANOVA supported a sex difference, particularly in pressure pain, as identified by means of unsupervised machine learning. Indeed, the highest statistical significance level among several significant sex differences in QST parameters (**Table 2**) was observed for PPT ($F = 34.43$, $P = 9.57·10^{-8}$).

4. Discussion

This study assessed established models of heat hyperalgesia with a variety of noxious stimuli, extending the original heat stimulation by the application of cold and mechanical stimuli. Considering the potential use of human experimental pain models for analgesic drug research, we applied a clinically established QST battery that was originally developed to phenotype neuropathic pain in patients, which was also successfully used in a human experimental context on healthy subjects.[18,45,46] To extract meaningful information from the resulting high-dimensional data, we applied machine-learning techniques with the aims of (1) identifying the most relevant effects of UV-B and topical capsaicin on QST parameters and (2) identifying possible subgroups of subjects who share similar QST responses to selected hypersensitization treatments. The results of these analyses indicated that (1) both UV-B– and capsaicin-induced experimental hypersensitization primarily increased subjects' sensitivity to heat; (2) UV-B additionally modulated sensitivity to cold; (3) subgroups of responders to topical application of capsaicin differed with respect to their sensitivity to pressure pain, and this could be attributed to sex differences; and (4) the response to the UV-B hypersensitization treatment was heterogeneous and included a group of nonresponders, which in the high-dimensional space of the QST pattern was indistinguishable from the absence of any hypersensitization treatment.
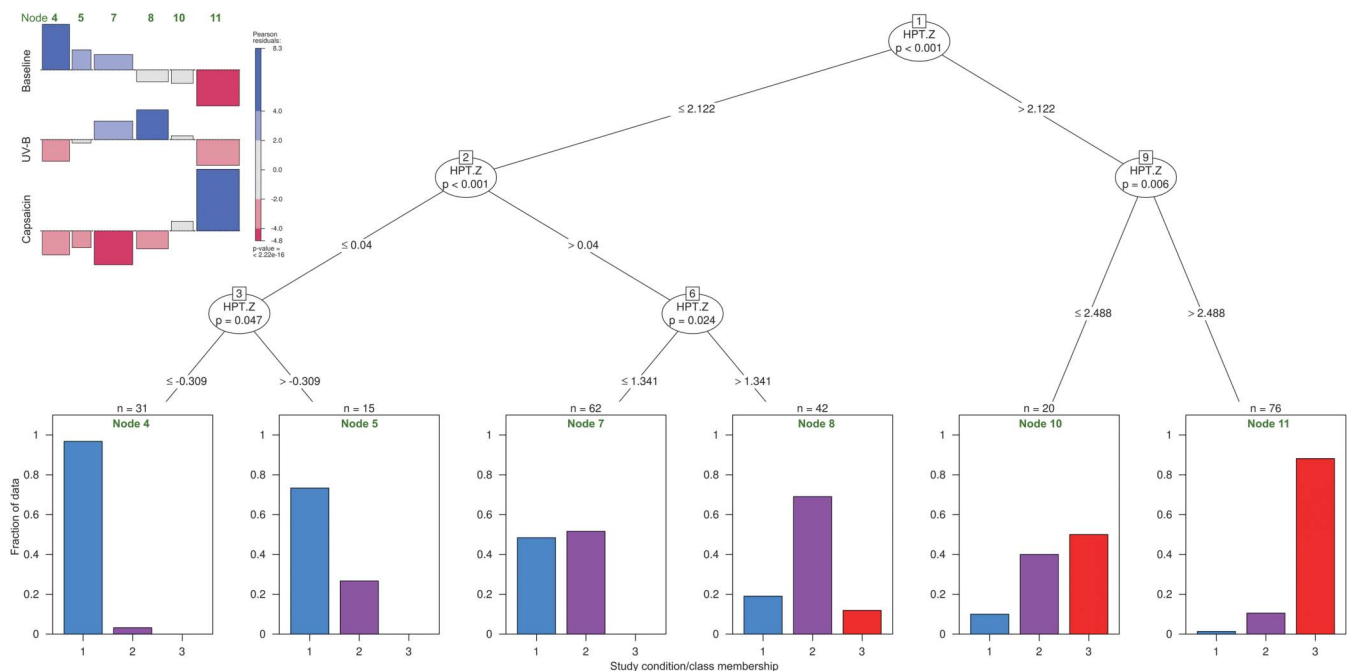
Figure 3. Decision tree associating ranges of the quantitative sensory testing (QST) parameter most affected by hypersensitization according to feature selection analysis (Fig. 2) with the 3 study conditions: baseline (1), ultraviolet-B (UV-B) (2), or capsaicin (3). The split criterion was the Gini impurity, and only statistically significant splits, based on permutation tests, were accepted. The tree ended in 6 terminal nodes (4, 5, 7, 8, 10, 11) at which the number of measurements assigned to the respective node is shown as bar plots, with separate bars for each study treatment (blue = baseline, violet = UV-B, red = capsaicin). Higher z-scores indicate higher sensitivity to the respective stimuli. At the upper left corner, an association plot is shown to visualize the residuals of an independence model for the contingency table.[14] Each cell of the contingency table is represented by a rectangle that has a height proportional to the contribution to Pearson χ for the cell and width proportional to the square root of expected counts corresponding to the cell. Hence, the area of each box is proportional to the difference in observed and expected frequencies. The rectangles in each row are positioned relative to a baseline indicating independence, ie, if the observed frequency of a cell is greater than the expected frequency, the box rises above the baseline, but otherwise it falls below it. Each study treatment (lines) is plotted vs the decision tree terminal nodes (columns) as a result of a contingency table analysis, indicating the relative representations of each treatment across the tree nodes. The Pearson residuals are colored according to a perceptually uniform hue-chroma-luminance (HCL) given at the right margin of the association plot.[52] The figure has been created using the R software package (version 3.3.3 for Linux; http://CRAN.R-project.org/, Ref. 68). Specifically, for drawing the tree and association plots, the "vcd" package (https://cran.r-project.org/package=vcd) was used[54] including the "strucplot" framework[53] and residual-based shadings.[97] HPT, heat pain threshold.

The present results are compatible with prior pathophysiological knowledge. Specifically, our results emphasize that both experimental pain models involve hypersensitization to heat stimuli as a major physiological mechanism. It has been recognized for decades that capsaicin excites TRPV1 ion channels,[84] and we have long known that TRPV1 is a heat sensor.[12] Similarly, UV irradiation has been shown to increase mRNAs level of TRPV1 by 2.4-fold in healthy subjects,[41] and more recent studies have shown that TRPV4 is involved in thermal sensation.[96] For both models, reports indicate the reversal of these hypersensitization effects by TRPV1 antagonists as novel analgesics under drug development.[3,11,73,76] However, UV-B radiation has been additionally shown to generate sunburn pain by activating epidermal TRPV4 ion channels, at least in mice,[57] which supports our observations that the 2 models share many similarities but are not identical in their effects on QST parameters.

In particular for UV-B, an effect on cold sensation was identified as a feature contributing to the correct association of a measurement with the treatment during which it had been acquired. This finding agrees with evidence from animal experiments that have shown an effect of cold stress on cultured keratinocytes from UV-B–injured skin.[61] Cooler temperatures increase sensitivity to UV-B radiation in embryos and larvae of the frog *Limnodynastes peronii*.[92] This finding is compatible with reported differences in UV-B– and capsaicin-induced hypersensitization that are claimed to affect the clinical translation of these models from

experimental human studies on the effects of analgesics, in particular those targeting neuropathic pain.[91] The involvement of cold sensitization might be an advantage with regard to understanding neuropathic pain, considering that cold sensitization–based models such as topical menthol application have been successfully used to show the effects of drugs established in the treatment of neuropathic pain, such as pregabalin.[1] From a human genetics perspective, a close relation between heat and cold sensitivity has been reported previously. First, the ion channels mentioned so far are temperature sensors,[63] but in another study, local capsaicin application was reported to affect cold sensation,[60] a finding that was interpreted as indicating interactions among TRP channels.[13] For example, TRPA1 channels are often co-expressed with heat-gated TRPV1 channels[49,78], and the transient receptor potential channels may act in concert,[22] including heterodimerization or oligomerization of TRPV1 with TRPV3 and TRPA1.[29] Thus, the effects on cold pain observed following hypersensitization procedures that apparently address heat pain are biologically plausible.

The results of our study indicate that machine learning both in a supervised and unsupervised manner, and in particular the latter implemented as ESOM/U*-matrix–based clustering, are suitable methods to analyze human experimental pain data. This indication is supported by the compatibility of key results with a classical ANOVA. Moreover, by including techniques of feature selection involving hierarchical components, we designed this analysis to identify the most relevant effects of the
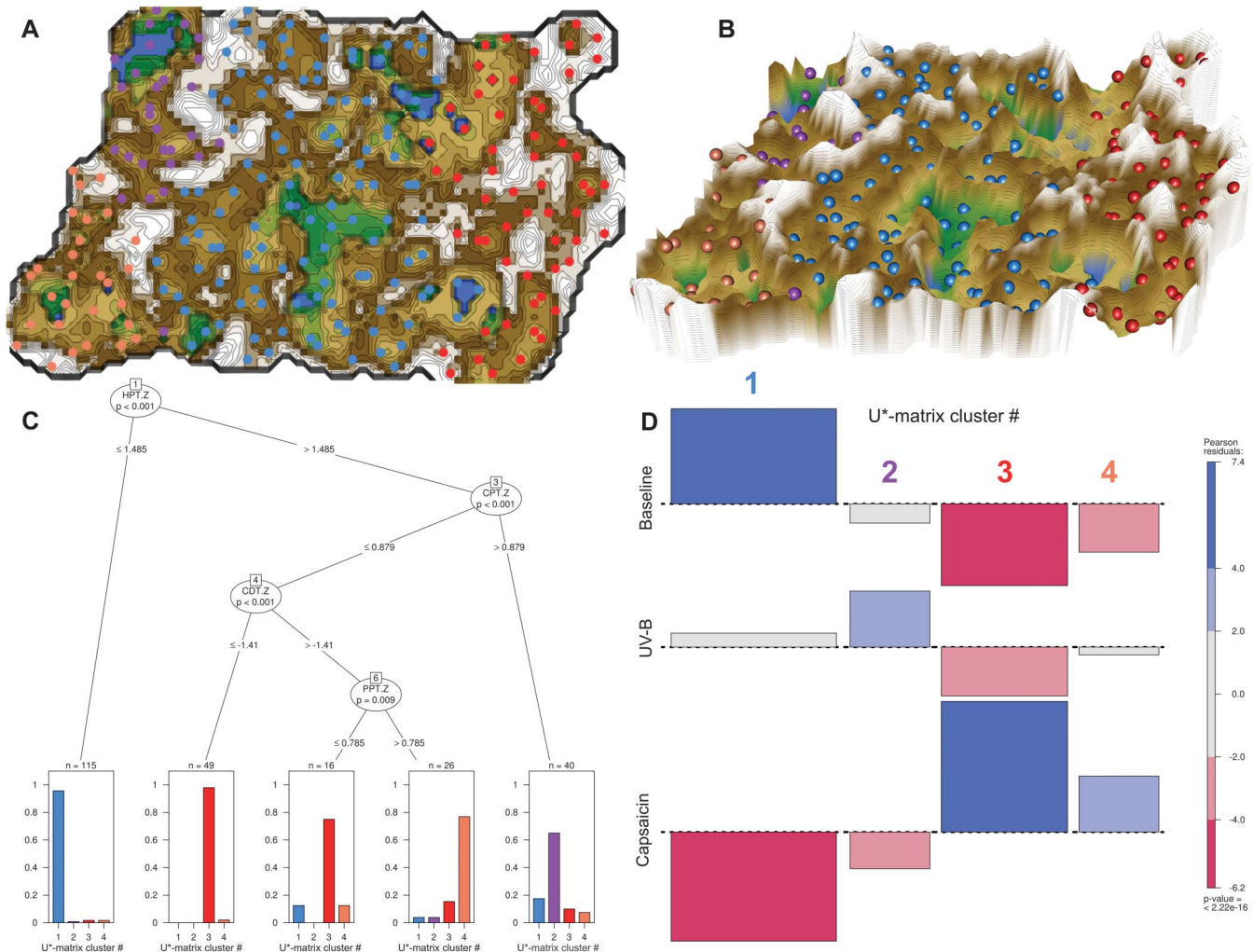
Figure 4. Machine-learned analysis aimed at detecting data structures of quantitative sensory testing (QST) parameter pattern acquired during the different study conditions (treatments). (A) U*-matrix visualization of distance- and density-based structures of the QST parameter pattern observed in 82 subjects under baseline conditions and following application of ultraviolet-B- or capsaicin-induced hypersensitization. The figure was created by projecting the data points onto a toroid grid of 4000 neurons where opposite edges are connected. The dots indicate the "best matching units" (BMUs) of the self-organizing map (SOM), which are those neurons whose weight vector is most similar to the input. A single neuron can be the BMU for more than 1 data point or subject; hence, the number of BMUs may not be equal to the number of acquired measurements. The U*-Matrix was colored as a geographical map with brown (up to snow-covered) heights and green valleys with blue lakes. Valleys indicate clusters and watersheds indicate borderlines between different clusters. The BMUs are colored according to the 4 clusters identified on the basis of this U*-matrix. (B) 3-D view of the same U*-star matrix, indicating cluster separation by "mountain ridges." (C) Decision tree associating emergent self-organizing feature map (ESOM)/U*-matrix–derived clusters with ranges of QST parameters. Higher z-scores indicate higher sensitivity to the respective stimuli. The split criterion was the Gini impurity, and only statistically significant splits, based on permutation tests, were accepted. The tree ended in 6 terminal nodes (4, 5, 7, 8, 10, 11) at which the number of measurements assigned to the respective node is shown as bar plots, with separate bars for each U*-matrix–based cluster. (D) Association plot visualizing the residuals of an independence model for the treatment vs clusters contingency table.[14] Each cell of the contingency table is represented by a rectangle that has height proportional to the contribution to Pearson χ for the cell and width proportional to the square root of expected counts corresponding to the cell. Hence, the area of each box is proportional to the difference in observed and expected frequencies. The rectangles in each row are positioned relative to a baseline indicating independence, ie, if the observed frequency of a cell is greater than the expected one, the box rises above the baseline, and falls below otherwise. Each study treatment (lines) is plotted vs the U*-matrix–derived clusters (columns) as a result of a contingency table analysis, indicating the relative representations of each cluster in across the tree nodes. The Pearson residuals are colored according to a perceptually uniform hue-chroma-luminance (HCL) given at the right margin of the association plot.[52] The figure was created using the R software package (version 3.3.3 for Linux; http://CRAN.R-project.org/, Ref. 68). Specifically, for drawing the tree and association plots, the "vcd" software package (https://cran.r-project.org/package=vcd) was used,[54] including the "strucplot" framework[53] and residual-based shadings.[97] HPT, heat pain threshold; PPT, pressure pain; CPT, cold pain threshold; CDT, cold detection threshold.

hypersensitization procedures on QST parameters, rather than to establish merely statistical significances of differences from baseline or between the 2 treatments. Specifically, the results of supervised learning emphasize that both sensitization procedures primarily modulate sensitivity to heat pain, which corresponds to the major involvement of TRPV1 and TRPV4 ion channels known as heat or thermal sensors.[12,96] This finding explains the degree of overlap observed in node 7 in **Figure 3**. Here, a possible dose effect might shift this overlap depending on

the relative doses of capsaicin and UV-B. In this study, capsaicin was standardized among subjects with respect to the dose applied, whereas UV-B was standardized with respect to the erythema effect obtained. Application of the same UV-B irradiation dose to all subjects could shift the hypersensitizing effect toward less overlap if a low dose was selected or toward more overlap if a high dose was selected, which must be taken into account when interpreting **Figure 3**. However, more pronounced effects of capsaicin on HPT as compared to those
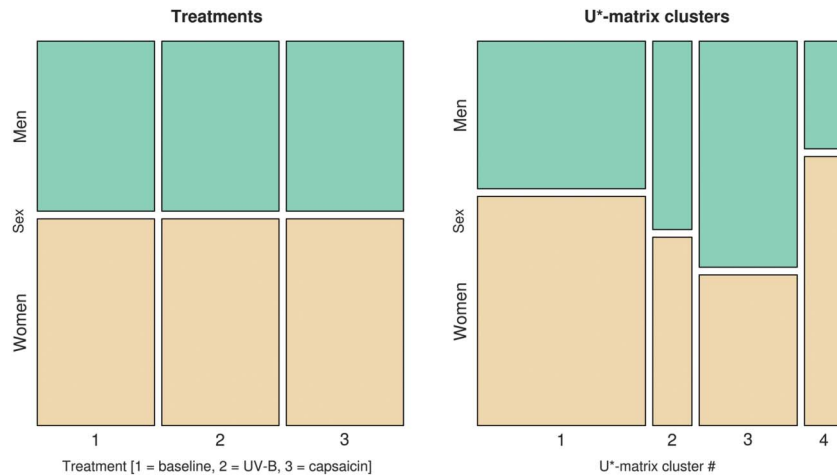
Figure 5. Analysis of the distribution of the subjects' sex across study treatments or clusters. The mosaic plots represent contingency tables of the sexes vs the study treatments (left) or the machine-learned clusters (right). The size of the cells as proportional to the number of subjects included. While sexes did not differ across treatments, the sex distribution across the emergent self-organizing feature map/U*-matrix–derived clusters (Fig. 4) was uneven at a statistical significance level of $P < 0.05$ (Fisher exact test). The figure has been created using the R software package (version 3.3.3 for Linux; http://CRAN.R-project.org/, Ref. 68). In particular, in U*-matrix–based clusters 3 vs 4 there were significantly more men or women, respectively ($P < 0.05$).

of UV-B would indicate the greater importance of TRPV1 than TRPV4 for heat sensation[12,96] at the molecular level.

Unsupervised machine learning followed a different approach, first identifying structures in the data of the whole study without reference to the study treatments. By contrast, the treatments emerged during data interpretation, aided by a further decision tree analysis. There, an additional importance of cold pain sensitivity came into play; however, this result is compatible with the findings of unsupervised learning. Indeed, in unsupervised learning the QST parameters cold detection threshold and cold pain threshold emerged in ABC set "B" (**Fig. 2A**) as important components of the decision tree exploring the clustering results of the ESOM (**Fig. 4**)

and were only neglected because of the predefined focus of that analysis to pay attention to only the most important parameters. Hence, the results of the different implementations of machine learning were compatible with each other.

The main focus of this analysis was data exploration for relevant effects of treatments or demographic parameters modulating the individual perception of pain to make them accessible to expert interpretation of the study results. The analysis was not aimed at creating a general-purpose classifier for capsaicin or UV-B effects because its application would be limited to a particular human experimental setting. Therefore, methods of further sophistication of the classifier methods were

Table 2

Results of analyses of variance for repeated measures (rm-ANOVA) with post hoc t tests vs baseline of the values acquired after ultraviolet-B (UV-B) or capsaicin treatments, performed for 10 quantitative sensory testing (QST) parameters; dynamic mechanical allodynia and paradoxical heat sensations were omitted owing to the absence of intersubject variation, and vibration detection threshold was omitted as it displayed only values (0 or 1) that did not change after application of the sensitization procedures.

QST parameter	ANOVA factor "treatment"*		ANOVA factor "sex"*		ANOVA interaction "treatment" by "sex"		t test† UV-B vs baseline		t test† capsaicin vs baseline		t test† UV-B vs capsaicin	
	F	P	F	P	F	P	T	P	T	P	T	P
CDT	110.35	**<2 × 10⁻¹⁶**	4.807	**0.0313**	1.062	0.348	0.085	1.00	−10.722	**<2 × 10⁻¹⁶**	10.807	**<2 × 10⁻¹⁶**
WDT	0.670	0.513	7.569	**0.00734**	0.059	0.943	0.228	1.00	0.984	0.98	−0.756	1.00
TSL	57.83	**<2 × 10⁻¹⁶**	7.468	**0.00773**	0.486	0.616	−0.085	1.00	−7.39	**7.1 × 10⁻¹²**	7.505	**1.2 × 10⁻¹¹**
CPT	145.23	**<2 × 10⁻¹⁶**	0.024	0.877	5.177	**0.00663**	−0.641	1.00	−9.494	**<2 × 10⁻¹⁶**	8.853	**5.4 × 10⁻¹⁶**
HPT	463.87	**<2 × 10⁻¹⁶**	12.21	**0.000777**	10.11	**7.33 × 10⁻⁵**	8.485	**6.4 × 10⁻¹⁵**	20.269	**<2 × 10⁻¹⁶**	−11.784	**<2 × 10⁻¹⁶**
PPT	15.35	**7.96 × 10⁻⁷**	34.43	**9.57 × 10⁻⁸**	1.376	0.255	2.174	0.092	1.543	0.372	0.631	1.00
MPT	18.54	**5.73 × 10⁻⁸**	24.51	**4.03 × 10⁻⁶**	2.586	0.0785	3.299	**0.0033**	2.362	0.0568	0.936	1.00
MPS	22.48	**2.48 × 10⁻⁹**	1.858	0.177	3.358	**0.0373**	1.793	0.22	1.583	0.34	0.21	1.00
WUR	13.31	**4.49 × 10⁻⁶**	2.064	0.155	1.081	0.342	2.589	**0.031**	2.034	0.129	0.555	1.00
MDT	8.07	**0.000458**	0.735	0.394	6.98	**0.001240**	2.463	**0.043**	−0.161	1.00	2.623	**0.028**

F and P values are shown for main effects and their interaction, with significant results marked in bold letters.
For the direction of the effects, see Figure 1.
* Degrees of freedom (df) = 2162.
† The α-correction was done within each analysis of variance separately, ie, for 3 post hoc tests.
CDT, cold detection threshold; CPT, cold pain threshold; HPT, heat pain threshold; MDT, mechanical detection threshold; MPS, mechanical pain sensitivity to pinprick stimuli; MPT, mechanical pain threshold; PPT, pressure pain threshold; TSL, thermal sensory limen; WDT, warm detection threshold; WUR, wind-up ratio.

not used, given the satisfactory results with respect to data interpretation. Such methods, however, may become important when classifiers of patients subgroups are addressed to provide a clinical diagnostic tool. In such projects, further cluster verification might become necessary. For example, it is known that different cluster algorithms may produce different results.[40] The present method seems to be comparatively robust in avoiding identification of false cluster structures in data.[88] A 20-fold repeated 80% resampling experiment delivered an average Rand Index[69] of 87.3% ± 3% for the coincidence of the subsampled clusters. More complex evaluations were not imperative, such as the addition of multiobjective clustering[25,40] or ensemble methods.[31]

The present analysis identified data structures that pointed at subgroups of subjects. One of the structural findings consisted of the identification of 2 separate clusters populated with measurements taken after topical capsaicin application. This distribution of the measurements taken under capsaicin-induced hypersensitization could be explained by a different sex distribution. In the cluster containing more women, higher pressure pain sensitivity was an important criterion of distinction from the other cluster, as indicated by the PPT-dependent node in the decision tree (**Fig. 4C**). This finding agrees with repeated reports of women's higher sensitivity to pressure pain.[19,36,37,42,59] It also agrees with most reports of the generally higher sensitivity to pain in women as compared to men (for reviews, see Refs. 5,6,16,70), which is also reflected in an overrepresentation of women among patients suffering from persistent pain.[56,74,94] The second subgroup was indirectly extrapolated from the fraction of measurements acquired following UV-B hypersensitization that nevertheless were dissolved in a cluster together with measurements taken during the baseline condition. This finding points at non-responders, for which the present data do not provide an explanation. Some obvious candidates are differences in the genes expressing TRPV1 or TRPV4, considering the involvement of these ion channels in the hypersensitization to UV-B discussed above; however, further TRP ion channels might be added.

5. Conclusions

In this study, we used machine-learning techniques for data exploration. Unsupervised machine learning, implemented as an ESOM/U*-matrix,[89] was able to depict the complete study on a single Kohonen map,[38] where the most relevant study results emerged. Combined with supervised machine learning implemented as random forest analysis,[9] the present analysis produced results that are biologically plausible, agree with previous knowledge, and are compatible with classical ANOVA results. Specifically, the present study indicates that both UV-B and capsaicin induce experimental hyperalgesia mainly toward noxious heat stimuli. In addition, UV-B seems to also modulate experimental hyperalgesia toward cold stimuli. Moreover, experimental hyperalgesia, in particular when induced by topical application of capsaicin, toward noxious blunt pressure stimuli displays a clear sex dependency, with women being more sensitive than men. Hence, while UV-B and capsaicin share a major component of heat pain sensitization, they clearly differ in their effects on the QST parameter patterns in healthy subjects, suggesting nonredundancy between these models, which should be kept in mind when using them concomitantly, rather than alternatively, in experimental human studies such as studies of analgesic drug effects.

Conflict of interest statement

Acknowledgements

References

[1] Altis K, Schmidtko A, Angioni C, Kuczka K, Schmidt H, Geisslinger G, Lötsch J, Tegeder I. Analgesic efficacy of tramadol, pregabalin and ibuprofen in menthol-evoked cold hyperalgesia. PAIN 2009;147:116–21.

[2] Altman DG, Bland JM. Diagnostic tests. 1: sensitivity and specificity. BMJ 1994;308:1552.

[3] Arendt-Nielsen L, Harris S, Whiteside GT, Hummel M, Knappenberger T, O'Keefe S, Kapil R, Kyle D. A randomized, double-blind, positive-controlled, 3-way cross-over human experimental pain study of a TRPV1 antagonist (V116517) in healthy volunteers and comparison with preclinical profile. PAIN 2016;157:2057–67.

[4] Baron R, Tölle TR, Gockel U, Brosz M, Freynhagen R. A cross-sectional cohort survey in 2100 patients with painful diabetic neuropathy and postherpetic neuralgia: differences in demographic data and sensory symptoms. PAIN 2009;146:34–40.

[5] Bartley EJ, Fillingim RB. Sex differences in pain: a brief review of clinical and experimental findings. Br J Anaesth 2013;111:52–8.

[6] Berkley KJ. Sex differences in pain. Behav Brain Sci 1997;20:371–80; discussion 435–513.

[7] Binder A, May D, Baron R, Maier C, Tölle TR, Treede RD, Berthele A, Faltraco F, Flor H, Gierthmuhlen J, Haenisch S, Huge V, Magerl W, Maihofner C, Richter H, Rolke R, Scherens A, Uceyler N, Ufer M, Wasner G, Zhu J, Cascorbi I. Transient receptor potential channel polymorphisms are associated with the somatosensory function in neuropathic pain patients. PLoS One 2011;6:e17387.

[8] Bonferroni CE. Teoria statistica delle classi e calcolo delle probabilita. Vol. 8. Florence, Italy: Pubblicazioni del R Istituto Superiore di Scienze Economiche e Commerciali di Firenze, 1936. p. 3–62.

[9] Breiman L. Random forests. Mach Learn 2001;45:5–32.

[10] Breimann L, Friedman JH, Olshen RA, Stone CJ. Classification and regression trees. Boca Raton: Chapman and Hall, 1993.

[11] Brown W, Leff RL, Griffin A, Hossack S, Aubray R, Walker P, Chiche DA. Safety, pharmacokinetic and pharmacodynamic study in healthy subjects of oral NEO6860, a modality selective TRPV1 antagonist. J Pain 2017;18: 726–38.

[12] Caterina MJ, Schumacher MA, Tominaga M, Rosen TA, Levine JD, Julius D. The capsaicin receptor: a heat-activated ion channel in the pain pathway. Nature 1997;389:816–24.

[13] Clapham DE, Runnels LW, Strubing C. The TRP ion channel family. Nat Rev Neurosci 2001;2:387–96.

[14] Cohen A. On the graphical display of the significant components in a two-way contingency table. Commun Stat Theory Methods 1980;A9: 1025–41.

[15] Dempster AP, Laird NM, Rubin DB. Maximum likelihood from incomplete data via the EM algorithm. J R Stat Soc Ser B 1977;39:1–38.

[16] Derbyshire SW. Gender, pain, and the brain. Pain Clinical Updates 2008; 16.

[17] Diatchenko L, Nackley AG, Slade GD, Bhalang K, Belfer I, Max MB, Goldman D, Maixner W. Catechol-O-methyltransferase gene

polymorphisms are associated with multiple pain-evoking stimuli. PAIN 2006;125:216–24.

[18] Dimova V, Oertel BG, Lötsch J. Using a standardized clinical quantitative sensory testing battery to judge the clinical relevance of sensory differences between adjacent body areas. Clin J Pain 2017;33:37–43.

[19] Doehring A, Küsener N, Fluhr K, Neddermeyer TJ, Schneider G, Lötsch J. Effect sizes in experimental pain produced by gender, genetic variants and sensitization procedures. PLoS One 2011;6:e17724.

[20] Efron B, Tibshirani RJ. An introduction to the bootstrap. San Francisco: Chapman and Hall, 1995.

[21] Fisher RA. On the interpretation of chi square from contingency tables, and the calculation of P. J R Stat Soc 1922;85:87–94.

[22] Guimaraes MZP, Jordt SE. TRPA1: a sensory channel of many talents. In: Liedtke WB, Heller S, editors. TRP ion channel function in sensory transduction and cellular signaling cascades. Boca Raton, FL: CRC Press/Taylor & Francis, 2007.

[23] Gustorff B, Anzenhofer S, Sycha T, Lehr S, Kress HG. The sunburn pain model: the stability of primary and secondary hyperalgesia over 10 hours in a crossover setting. Anesth Analg 2004;98:173–7; Table of contents.

[24] Guyon I, Elisseeff A. An introduction to variable and feature selection. J Mach Learn Res 2003;3:1157–82.

[25] Handl J, Knowles J. An evolutionary approach to multiobjective clustering. IEEE Trans Evol Comput 2007;11:56–76.

[26] Handwerker HO, Kobal G. Psychophysiology of experimentally induced pain. PhysiolRev 1993;73:639–71.

[27] Harrison GI, Young AR, McMahon SB. Ultraviolet radiation-induced inflammation as a model for cutaneous hyperalgesia. J Invest Dermatol 2004;122:183–9.

[28] Hastie BA, Riley JL III, Robinson ME, Glover T, Campbell CM, Staud R, Fillingim RB. Cluster analysis of multiple experimental pain modalities. PAIN 2005;116:227–37.

[29] Ho KW, Ward NJ, Calkins DJ. TRPV1: a stress response protein in the central nervous system. Am J Neurodegener Dis 2012;1:1–14.

[30] Hoffmann RT, Schmelz M. Time course of UVA- and UVB-induced inflammation and hyperalgesia in human skin. Eur J Pain 1999;3:131–9.

[31] Hornik K, Leisch F. Ensemble methods for cluster analysis. In: Taudes A, editor. Adaptive information systems and modelling in economics and management science. Vienna: Springer Vienna, 2005. p. 261–8.

[32] Hothorn T, Hornik K, Zeileis A. Unbiased recursive partitioning: a conditional inference framework. J Comput Graphical Stat 2006;15: 651–74.

[33] Jacoby WG. The dot plot: a graphical display for labeled quantitative values. The Pol Methodologist 2006;14:6–14.

[34] Julius D, Basbaum AI. Molecular mechanisms of nociception. Nature 2001;413:203–10.

[35] Juran JM. The non-pareto principle; mea culpa. Qual Prog 1975;8:8–9.

[36] Karshikoff B, Jensen KB, Kosek E, Kalpouzos G, Soop A, Ingvar M, Olgart Höglund C, Lekander M, Axelsson J. Why sickness hurts: a central mechanism for pain induced by peripheral inflammation. Brain Behav Immun 2016;57:38–46.

[37] Karshikoff B, Lekander M, Soop A, Lindstedt F, Ingvar M, Kosek E, Olgart Höglund C, Axelsson J. Modality and sex differences in pain sensitivity during human endotoxemia. Brain Behav Immun 2015;46:35–43.

[38] Kohonen T. Self-organized formation of topologically correct feature maps. Biol Cybernet 1982;43:59–69.

[39] Kohonen T. Self-organizing maps. Berlin: Springer, 1995.

[40] Kraus JM, Müssel C, Palm G, Kestler HA. Multi-objective selection for collecting cluster alternatives. Comput Stat 2011;26:341–53.

[41] Lee YM, Kim YK, Chung JH. Increased expression of TRPV1 channel in intrinsically aged and photoaged human skin in vivo. Exp Dermatol 2009; 18:431–6.

[42] Lemming D, Borsbo B, Sjors A, Lind EB, Arendt-Nielsen L, Graven-Nielsen T, Gerdle B. Cuff pressure pain detection is associated with both sex and physical activity level in nonathletic healthy subjects. Pain Med 2017. doi: 10.1093/pm/pnw309 [epub ahead of print].

[43] Lerch F. Bestimmung von gaussmixturmodellen durch einen evolutionären algorithmus und den chi quadrat test. Faculty of mathematics and computer science. Marburg: Philipps University Marburg, 2016. p. 101.

[44] Liaw A, Wiener M. Classification and regression by random forest. R News 2002;2:18–22.

[45] Lötsch J, Dimova V, Hermens H, Zimmermann M, Geisslinger G, Oertel BG, Ultsch A. Pattern of neuropathic pain induced by topical capsaicin application in healthy subjects. PAIN 2015;156:405–14.

[46] Lötsch J, Dimova V, Ultsch A, Lieb I, Zimmermann M, Geisslinger G, Oertel BG. A small yet comprehensive subset of human experimental pain models emerging from correlation analysis with a clinical quantitative sensory testing protocol in healthy subjects. Eur J Pain 2016;20:777–89.

[47] Lötsch J, Ultsch A. Exploiting the structures of the U-matrix. In: Villmann T, Schleif FM, Kaden M, Lange M, editors. Advances in intelligent systems and computing. Vol. 295. Heidelberg: Springer, 2014. p. 248–57.

[48] Magerl W, Krumova EK, Baron R, Tolle T, Treede RD, Maier C. Reference data for quantitative sensory testing (QST): refined stratification for age and a novel method for statistical comparison of group data. PAIN 2010; 151:598–605.

[49] Malin S, Molliver D, Christianson JA, Schwartz ES, Cornuet P, Albers KM, Davis BM. TRPV1 and TRPA1 function and modulation are target tissue dependent. J Neurosci 2011;31:10516–28.

[50] McGrayne SB. The theory that would not die: how Bayes' rule cracked the enigma code, hunted down Russian submarines & emerged triumphant from two centuries of controversy. New Haven: Yale University Press, 2011.

[51] Metz CE. Basic principles of ROC analysis. Semin Nucl Med 1978;8: 283–98.

[52] Meyer D, Zeileis A, Hornik K. Visualizing independence using extended association plots. Proceedings of the 3rd International Workshop on Distributed Statistical Computing. March 20–22 2003, Vienna, Austria, 2003.

[53] Meyer D, Zeileis A, Hornik K. The strucplot framework: visualizing multi-way contingency tables with vcd. J Stat Softw 2006;17:1–48.

[54] Meyer D, Zeileis A, Hornik K. VCD: visualizing categorical data, 2016. https://cran.r-project.org/web/packages/vcd/.

[55] Mogil JS. The genetic mediation of individual differences in sensitivity to pain and its inhibition. Proc Natl Acad Sci U S A 1999;96:7744–51.

[56] Mogil JS. Sex differences in pain and pain inhibition: multiple explanations of a controversial phenomenon. Nat Rev Neurosci 2012;13:859–66.

[57] Moore C, Cevikbas F, Pasolli HA, Chen Y, Kong W, Kempkes C, Parekh P, Lee SH, Kontchou NA, Yeh I, Jokerst NM, Fuchs E, Steinhoff M, Liedtke WB. UVB radiation generates sunburn pain and affects skin by activating epidermal TRPV4 ion channels and triggering endothelin-1 signaling. Proc Natl Acad Sci U S A 2013;110:E3225–34.

[58] Murphy KP. Machine learning: a probabilistic perspective. Cambridge, MA: The MIT Press, 2012.

[59] Neziri AY, Scaramozzino P, Andersen OK, Dickenson AH, Arendt-Nielsen L, Curatolo M. Reference values of mechanical and thermal pain tests in a pain-free population. Eur J Pain 2011;15:376–83.

[60] Nolano M, Simone DA, Wendelschafer-Crabb G, Johnson T, Hazen E, Kennedy WR. Topical capsaicin in humans: parallel loss of epidermal nerve fibers and pain sensation. PAIN 1999;81:135–45.

[61] Ota T, Hanada K, Hashimoto I. The effect of cold stress on UVB injury in mouse skin and cultured keratinocytes. Photochem Photobiol 1996;64: 984–7.

[62] Pareto V. Manuale di economia politica, Milan: società editrice libraria, revised and translated into French as manuel d'économie politique. Paris: Giard et Briére, 1909.

[63] Patapoutian A, Peier AM, Story GM, Viswanath V. ThermoTRP channels and beyond: mechanisms of temperature sensation. Nat Rev Neurosci 2003;4:529–39.

[64] Pearson K. On the criterion that a given system of deviations from the probable in the case of a correlated system of variables is such that it can be reasonably supposed to have arisen from random sampling. Philosophical Magazine Series 5 1900;50:157–75.

[65] Petersen KL, Rowbotham MC. A new human experimental pain model: the heat/capsaicin sensitization model. Neuroreport 1999;10:1511–16.

[66] Pfau D, Klein T, Blunk JA, Geber C, Krumova E, Limbeck C, Magerl W, Maier C, Westermann A, Schuh-Hofer S, Tiede W, Treede RD. QST Quantitative sensorische Testung, Handanweisung für den Untersucher, Eine standardisierte Testbatterie für die Quantitative Sensorische Testung nach den Regeln des Deutschen Forschungsverbundes Neuropathischer Schmerz (DFNS). In: Rolke R, Andrews A, Magerl W, Treede RD, editors: Lehrstuhl für Neurophysiologie, Universitätsmedizin Mannheim, Germany: 2010.

[67] President's Information Technology Advisory C. Report to the president: computational science: ensuring America's competitiveness. Arlington, VA: National Coordination Office for Information Technology Research and Development, 2005. http://www.nitrd.gov3.

[68] R Development Core Team. R: a language and environment for statistical computing. Vienna, 2008.

[69] Rand WM. Objective criteria for the evaluation of clustering methods. J Am Stat Assoc 1971;66:846–50.

[70] Riley JL III, Robinson ME, Wise EA, Myers CD, Fillingim RB. Sex differences in the perception of noxious experimental stimuli: a meta-analysis. PAIN 1998;74:181–7.

[71] Rolke R, Baron R, Maier C, Tölle TR, Treede RD, Beyer A, Binder A, Birbaumer N, Birklein F, Botefur IC, Braune S, Flor H, Huge V, Klug R, Landwehrmeyer GB, Magerl W, Maihofner C, Rolko C, Schaub C, Scherens A, Sprenger T, Valet M, Wasserka B. Quantitative sensory

testing in the German research network on neuropathic pain (DFNS): standardized protocol and reference values. PAIN 2006;123:231–43.

[72] Rolke R, Magerl W, Campbell KA, Schalber C, Caspari S, Birklein F, Treede RD. Quantitative sensory testing: a comprehensive protocol for clinical trials. Eur J Pain 2006;10:77–88.

[73] Rowbotham MC, Nothaft W, Duan WR, Wang Y, Faltynek C, McGaraughty S, Chu KL, Svensson P. Oral and cutaneous thermosensory profile of selective TRPV1 inhibition by ABT-102 in a randomized healthy volunteer trial. PAIN 2011;152:1192–200.

[74] Ruau D, Liu LY, Clark JD, Angst MS, Butte AJ. Sex differences in reported pain across 11,000 patients captured in electronic medical records. J Pain 2012;13:228–34.

[75] Saeys Y, Inza I, Larranaga P. A review of feature selection techniques in bioinformatics. Bioinformatics 2007;23:2507–17.

[76] Schaffler K, Reeh P, Duan WR, Best AE, Othman AA, Faltynek CR, Locke C, Nothaft W. An oral TRPV1 antagonist attenuates laser radiant-heat-evoked potentials and pain ratings from UV(B)-inflamed and normal skin. Br J Clin Pharmacol 2013;75:404–14.

[77] Schaible HG, Richter F. Pathophysiology of pain. Langenbecks Arch Surg 2004;389:237–43.

[78] Story GM, Peier AM, Reeve AJ, Eid SR, Mosbacher J, Hricik TR, Earley TJ, Hergarden AC, Andersson DA, Hwang SW, McIntyre P, Jegla T, Bevan S, Patapoutian A. ANKTM1, a TRP-like channel expressed in nociceptive neurons, is activated by cold temperatures. Cell 2003;112:819–29.

[79] Student. The probable error of a mean. Biometrika 1908;6:1–25.

[80] Sycha T, Gustorff B, Lehr S, Tanew A, Eichler HG, Schmetterer L. A simple pain model for the evaluation of analgesic effects of NSAIDs in healthy subjects. Br J Clin Pharmacol 2003;56:165–72.

[81] Thrun MC, Lerch F, Lötsch J, Ultsch A. Visualization and 3D printing of multivariate data of biomarkers. In: Skala V, editor. International conference in central Europe on computer graphics, visualization and computer vision (WSCG). Vol. 24. Czech Republic: Plzen, 2016.

[82] Thrun MC, Lerch F, Lötsch J, Ultsch A. Visualization and 3D printing of multivariate data of biomarkers. Proceedings of International Conference in Central Europe on Computer Graphics, Visualization and Computer Vision. Plzen, Czech Republic; May 29–June 2, 2017. pp. 7–16.

[83] Tillé Y, Matei A. The R sampling package. Presented at Software demonstration at The Fifth International Conference on Establishment Surveys (ICES-V), Geneva, 2016.

[84] Tominaga M, Caterina MJ, Malmberg AB, Rosen TA, Gilbert H, Skinner K, Raumann BE, Basbaum AI, Julius D. The cloned capsaicin receptor integrates multiple pain-producing stimuli. Neuron 1998;21:531–43.

[85] Ultsch A. Maps for visualization of high-dimensional data spaces. Proceedings of the WSOM, Kyushu, Japan, 2003. pp. 225–30.

[86] Ultsch A. Pareto density estimation: a density estimation for knowledge discovery. In: Baier D, Werrnecke KD, editors, Proceedings of the innovations in classification, datascience, and information systems—proceedings 27th Annual Conference of the German Classification Society (GfKL). Heidelberg, Germany: Springer, 2003.

[87] Ultsch A, Lötsch J. Computed ABC analysis for rational selection of most informative variables in multivariate data. PLoS One 2015;10: e0129767.

[88] Ultsch A, Lötsch J. Machine-learned cluster identification in high-dimensional data. J Biomed Inform 2017;66:95–104.

[89] Ultsch A, Sieman HP. Kohonen's self organizing feature maps for exploratory data analysis, proceedings of the INNC'90, Int Neural Network Conference. Alphen aan den Rijn, the Netherlands: Kluwer, 1990. p. 305–8.

[90] Ultsch A, Thrun MC, Hansen-Goos O, Lötsch J. Identification of molecular fingerprints in human heat pain thresholds by use of an interactive mixture model R toolbox (AdaptGauss). Int J Mol Sci 2015;16: 25897–911.

[91] van Amerongen G, de Boer MW, Groeneveld GJ, Hay JL. A literature review on the pharmacological sensitivity of human evoked hyperalgesia pain models. Br J Clin Pharmacol 2016;82:903–22.

[92] Van Uitregt VO, Wilson RS, Franklin CE. Cooler temperatures increase sensitivity to ultraviolet B radiation in embryos and larvae of the frog Limnodynastes peronii. Glob Change Biol 2007;13:1114–21.

[93] Varma S, Simon R. Bias in error estimation when using cross-validation for model selection. BMC Bioinformatics 2006;7:91.

[94] Westergren H, Larsson J, Freeman M, Carlsson A, Jöud A, Malmström E-M. Sex-based differences in pain distribution in a cohort of patients with persistent post-traumatic neck pain. Disabil Rehabil 2017:1–10. doi: 10.1080/09638288.2017.1280543 [Epub ahead of print].

[95] Woolf CJ, Mannion RJ. Neuropathic pain: aetiology, symptoms, mechanisms, and management. Lancet 1999;353:1959–64.

[96] Yatsu R, Miyagawa S, Kohno S, Saito S, Lowers RH, Ogino Y, Fukuta N, Katsu Y, Ohta Y, Tominaga M, Guillette LJ Jr, Iguchi T. TRPV4 associates environmental temperature and sex determination in the American alligator. Sci Rep 2015;5:18581.

[97] Zeileis A, Meyer D, Hornik K. Residual-based shadings for visualizing (conditional) independence. J Comput Graphical Stat 2007;16:507–25.